

# ALMA AND GMRT CONSTRAINTS ON THE OFF-AXIS GAMMA-RAY BURST 170817A FROM THE BINARY NEUTRON STAR MERGER GW170817

S. KIM,<sup>1,2</sup> S. SCHULZE,<sup>3</sup> L. RESMI,<sup>4</sup> J. GONZÁLEZ-LÓPEZ,<sup>1</sup> A. B. HIGGINS,<sup>5</sup> C. H. ISHWARA-CHANDRA,<sup>6</sup> F. E. BAUER,<sup>1,7,8</sup> I. DE GREGORIO-MONSALVO,<sup>9,10</sup> M. DE PASQUALE,<sup>11</sup> A. DE UGARTE POSTIGO,<sup>12</sup> D. A. KANN,<sup>12</sup> S. MARTÍN,<sup>9,10</sup> S. R. OATES,<sup>13</sup> R. L. C. STARLING,<sup>5</sup> S. CAMPANA,<sup>14</sup> Z. CANO,<sup>12</sup> S. COVINO,<sup>14</sup> A. S. FRUCHTER,<sup>15</sup> J. P. U. FYNBO,<sup>16</sup> D. H. HARTMANN,<sup>17</sup> J. HJORTH,<sup>18</sup> P. JAKOBSSON,<sup>19</sup> A. J. LEVAN,<sup>13</sup> D. MALESANI,<sup>18</sup> M. J. MICHAŁOWSKI,<sup>20</sup> B. MILVANG-JENSEN,<sup>18</sup> K. MISRA,<sup>21</sup> R. SÁNCHEZ-RAMÍREZ,<sup>22</sup> N. R. TANVIR,<sup>5</sup> C. C. THÖNE,<sup>12</sup> D. J. WATSON,<sup>16</sup> AND K. WIERSEMA<sup>13</sup>

<sup>1</sup>*Instituto de Astrofísica and Centro de Astroingeniería, Facultad de Física, Pontificia Universidad Católica de Chile, Casilla 306, Santiago 22, Chile*

<sup>2</sup>*Max-Planck-Institut für Astronomie Königstuhl 17 D-69117 Heidelberg, Germany*

<sup>3</sup>*Department of Particle Physics and Astrophysics, Weizmann Institute of Science, Rehovot 761000, Israel*

<sup>4</sup>*Indian Institute of Space Science & Technology, Trivandrum 695547, India*

<sup>5</sup>*Department of Physics and Astronomy, University of Leicester, University Road, Leicester, LE1 7RH, United Kingdom*

<sup>6</sup>*National Center for Radio Astrophysics, Pune 411007, India*

<sup>7</sup>*Millennium Institute of Astrophysics (MAS), Nuncio Monseñor Sótero Sanz 100, Providencia, Santiago, Chile*

<sup>8</sup>*Space Science Institute, 4750 Walnut Street, Suite 205, Boulder, Colorado 80301, USA*

<sup>9</sup>*European Southern Observatory, Alonso de Córdova 3107, Vitacura, Santiago 763-0355, Chile*

<sup>10</sup>*Joint ALMA Observatory, Alonso de Córdova 3107, Vitacura, Santiago 763-0355, Chile*

<sup>11</sup>*Department of Astronomy and Space Sciences, Istanbul University, 34119 Beyazıt, Istanbul, Turkey*

<sup>12</sup>*Instituto de Astrofísica de Andalucía (IAA-CSIC), Glorieta de la Astronomía, s/n, 18008, Granada, Spain*

<sup>13</sup>*Department of Physics, University of Warwick, Coventry, CV4 7AL, United Kingdom*

<sup>14</sup>*INAF - Osservatorio astronomico di Brera, Via E. Bianchi 46, 23807, Merate (LC), Italy*

<sup>15</sup>*Space Telescope Science Institute, 3700 San Martin Dr., Baltimore, MD 21218*

<sup>16</sup>*Niels Bohr Institute, University of Copenhagen, Juliane Maries Vej 30, DK-2100 Copenhagen Ø, Denmark*

<sup>17</sup>*Department of Physics and Astronomy, Clemson University, Clemson, SC 29634-0978, USA*

<sup>18</sup>*Dark Cosmology Centre, Niels Bohr Institute, University of Copenhagen, Juliane Maries Vej 30, DK-2100 Copenhagen Ø, Denmark*

<sup>19</sup>*Centre for Astrophysics and Cosmology, Science Institute, University of Iceland, Dunhagi 5, 107 Reykjavík, Iceland*

<sup>20</sup>*Astronomical Observatory Institute, Faculty of Physics, Adam Mickiewicz University, ul. Słoneczna 36, 60-286 Poznań, Poland*

<sup>21</sup>*Aryabhata Research Institute of observational scienceES (ARIES), Manora Peak, Nainital 263 001, India*

<sup>22</sup>*INAF, Istituto Astrofisica e Planetologia Spaziali, Via Fosso del Cavaliere 100, I-00133 Roma, Italy*

## ABSTRACT

Binary neutron-star mergers (BNSMs) are among the most readily detectable gravitational-wave (GW) sources with LIGO. They are also thought to produce short  $\gamma$ -ray bursts (SGRBs), and kilonovae that are powered by r-process nuclei. Detecting these phenomena simultaneously would provide an unprecedented view of the physics during and after the merger of two compact objects. Such a Rosetta Stone event was detected by LIGO/Virgo on 17 August 2017 at a distance of  $\sim 40$  Mpc. We monitored the position of the BNSM with ALMA at 338.5 GHz and GMRT at 1.4 GHz, from 1.4 to 44 days after the merger. Our observations rule out any afterglow more luminous than  $3 \times 10^{26}$  erg s<sup>-1</sup> in these bands, probing  $>2$ – $4$  dex fainter than previous SGRB limits. We match these limits, in conjunction with public data announcing the appearance of X-ray and radio emission in the weeks after the GW event, to templates of off-axis afterglows. Our broadband modeling suggests that GW170817 was accompanied by a SGRB and that the GRB jet, powered by  $E_{\text{AG, iso}} \sim 10^{50}$  erg, had a half-opening angle of  $\sim 20^\circ$ , and was misaligned by  $\sim 41^\circ$  from our line of sight. The data are also consistent with a more powerful, collimated jet:  $E_{\text{AG, iso}} \sim 10^{51}$  erg,  $\theta_{1/2, \text{jet}} \sim 5^\circ$ ,  $\theta_{\text{obs}} \sim 17^\circ$ . This is the most conclusive detection of an off-axis GRB afterglow and the first associated with a BNSM-GW event to date. We use the viewing angle estimates to infer the initial bulk Lorentz factor and true energy release of the burst.

*Keywords:* gravitational waves: GW170817 gamma-ray burst: GRB 170817A

## 1. INTRODUCTION

The existence of gravitational waves (GWs) was predicted in 1916 (Einstein 1916, 1918), but it took almost a century to directly observe them (Abbott et al. 2016). Some of the GW signals readily detectable with the Laser Interferometer Gravitational-wave Observatory (LIGO) are linked to the coalescence of two neutron stars (Abadie et al. 2010). This class of object is also thought to be the progenitor of short gamma-ray bursts (SGRBs; duration  $\lesssim 2$  s; Eichler et al. 1989; Nakar 2007; Berger 2014). In addition, the temperatures and densities in the debris of the merger are thought to be high enough to also produce radioactive nuclei through rapid neutron capture. Their decays could give rise to faint supernova-like transients, called kilonovae (KNe) (e.g., Li & Paczyński 1998; Rosswog 2005; Kasen et al. 2013, for a review see also Metzger 2017). Observational evidence for a KN was found in the near-IR photometry of SGRB 130603B (Tanvir et al. 2013) and possibly in optical photometry of GRBs 050709 and 060614 (Jin et al. 2015, 2016). However, without a spectrum, the conjecture that SGRBs are accompanied by KNe and therefore that SGRBs are connected with binary neutron star mergers (BNSMs) is not free of ambiguity.

On 17 August 2017 at 12:41:04 UTC, the joint LIGO and Virgo observing run detected a BNSM at  $40^{+8}_{-14}$  Mpc within an area of  $28 \text{ deg}^2$  projected on the sky (LIGO Scientific Collaboration & Virgo Collaboration 2017b). The precise distance and localization gave the follow-up with optical wide-field imagers a flying start (for a comprehensive review see LIGO Scientific Collaboration et al. 2017). Coulter et al. (2017) targeted galaxies at this distance and detected a new object, SSS17a, at  $\alpha_{J2000} = 13^{\text{h}}09^{\text{m}}48^{\text{s}}.09$ ,  $\delta_{J2000} = -23^{\circ}22'53''.3$ ;  $10''.3$  from NGC 4993 at 43.9 Mpc ( $z = 0.00984$ ; Levan et al. 2017, For a detailed discussion see also Hjorth et al. 2017).<sup>1</sup> This discovery was confirmed by several teams including Allam et al. (2017), Melandri et al. (2017), Tanvir & Levan (2017) and Yang et al. (2017). The transient rapidly faded in the optical, but showed a much slower evolution in the near-IR (Tanvir et al. 2017a). Spectra of SSS17a revealed very broad absorption features, due to relativistic expansion velocities (Pian et al. 2017; Smartt et al. 2017; Tanvir et al. 2017a), similar to that expected for KNe (Kasen et al. 2013; Tanaka et al. 2014). Such features are unlike any known for supernovae spectra and strongly argued for a connection between SSS17 and GW170817.

The GBM detector aboard the  $\gamma$ -ray satellite *Fermi* (Blackburn et al. 2017; von Kienlin et al. 2017; Goldstein

et al. 2017a,b) as well as *INTEGRAL* (Savchenko et al. 2017b,a) detected a faint 2-s duration GRB (hereafter GRB 170817A), 1.7 s after GW170817 (LIGO Scientific Collaboration & Virgo Collaboration 2017b). Although the chance coincidence is very small to find both transients quasi-contemporaneous and in the same region of the sky, the credible region of the  $\gamma$ -ray localization had a size of  $\sim 1100 \text{ deg}^2$  (90% confidence; Blackburn et al. 2017). To firmly establish the connection between GRB 170817A and GW170817 by detecting the afterglow of the GRB in the X-ray and radio bands, numerous groups carried out large follow-up campaigns to very deep limits, but without success (e.g. Alexander et al. 2017; Bannister et al. 2017; Cenko et al. 2017; Corsi et al. 2017e; De et al. 2017; Deller et al. 2017; Evans et al. 2017; Kaplan et al. 2017; Margutti et al. 2017; Resmi et al. 2017; Sugita et al. 2017). Not until nine days after GW170817 a brightening X-ray source was detected at the position of SSS17a (Troja et al. 2017). Subsequent X-ray observations confirmed the brightening (Fong et al. 2017; Haggard et al. 2017b). About a week later, Corsi et al. (2017c) and Mooley et al. (2017a) detected an emerging radio source at 3 and 6 GHz as well. While these observations might support the SGRB connection, such a behavior is highly atypical for GRB afterglows (e.g., Piran 2004).

In this letter, we examine the afterglow properties of SSS17a. We present sub-mm and radio observations obtained with the Atacama Large Millimeter/submillimeter Array (ALMA) and the Giant Metrewave Radio Telescope (GMRT) between 1.4 and 44.1 days after the GW detection. We augment our dataset with public X-ray, optical, and radio data and confront GRB afterglow models with observations.

All uncertainties reported in this paper are given at  $1\sigma$  confidence. Non-detections are reported at  $3\sigma$  confidence, unless stated otherwise.

## 2. OBSERVATIONS AND DATA REDUCTION

We observed the field of SSS17a as a part of the observing program 2016.1.00862.T (P.I. Kim) with ALMA in the Atacama desert (Chile; Wootten & Thompson 2009) and as part of the Director's Discretionary Time (DDT) Proposal DDTB285 with the GMRT, Pune (India; P.I. Resmi; Swarup et al. 1991).

### 2.1. ALMA observations

Our initial ALMA campaign started on 18 August 2017 at 22:50:40 UTC (1.4 days after GW170817) and lasted for eight days (Schulze et al. 2017). In addition, we secured a final epoch  $\sim 44$  days after GW170817. In total, we obtained six epochs at 338.5 GHz (Table 1). The integration time of each observation was set to reach a nominal r.m.s. of  $\sim 40 \mu\text{Jy/beam}$ . The initial ALMA observations were performed in the C40-7 configuration, with a field of view

<sup>1</sup> The luminosity distance was derived for a flat  $\Lambda$ CDM cosmology with  $\Omega_m = 0.315$ ,  $\Omega_\Lambda = 0.685$ ,  $H_0 = 67.3 \text{ km s}^{-1} \text{ Mpc}^{-1}$  (Planck Collaboration. XVI. 2014). We will use this cosmology throughout the paper.

of  $18.''34$  in diameter and an average synthesized beam of  $\approx 0.''13 \times 0.''07$ . The observation at 44 days after GW170817 was performed in the most extended ALMA configuration, C40-8/9, yielding a synthesized beam of  $0.''026 \times 0.''016$ .

The ALMA data were reduced with scripts provided by ALMA and with the software package COMMON ASTRONOMY SOFTWARE APPLICATIONS (CASA) version 4.7.2 (McMullin et al. 2007).<sup>2</sup> For each epoch, we created images using TCLEAN, with a pixel size of  $0.''01/\text{px}$ . We interactively selected cleaning regions around detected sources (none corresponding to the SSS17a counterpart). The cleaning process was repeated until no clear emission was left. The r.m.s. was measured in a  $10''$ -width box around the central position in the images without primary beam correction.

No significant signal is detected at the position of SSS17a. Table 1 summarizes the  $3\sigma$  detection limits. The galaxy nucleus is well detected and marginally resolved in our data ( $\alpha, \delta$  (J2000) =  $13^{\text{h}}09^{\text{m}}47.6975^{\text{s}}, -23^{\circ}23'02.''3788$ ). We measure  $1.07 \pm 0.21$  mJy at 338.5 GHz. In addition, we detect a marginally resolved sub-mm galaxy with  $F_{338.5\text{ GHz}} = 1.15 \pm 0.21$  mJy at  $\alpha, \delta$  (J2000) =  $13^{\text{h}}09^{\text{m}}48.3990^{\text{s}}, -23^{\circ}22'48.''2920$ . The quasars J1337–1257 and J1427–4206 were used for band and flux calibration, and J1256–2547, J1937–3958, and J1258–2219 for phase calibration.

## 2.2. GMRT Observations

The GMRT is one of the most sensitive low-frequency radio telescopes in operation currently. It operates at low radio frequencies from 150 MHz to 1.4 GHz (Swarup et al. 1991). We secured three epochs in the L band, centered at 1.39 GHz, between 25 August 2017 and 16 September 2017 (i.e., between 7.9 and 29.8 days since GW170817; Table 1; Resmi et al. 2017). The on-source integration time was  $\sim 1.5$  hr for each observation. The first epoch was performed with the new 200-MHz correlator that divides the bandpass into 2048 channels of which  $\sim 70\%$  were usable, due to radio frequency interference. The second and the third epoch were performed with the 32-MHz correlator. The synthesized beam sizes were typically  $4'' \times 2''$ . The quasar 3C286 was used as flux and bandpass calibrator and J1248–199 was used for phase and additional bandpass calibration. Data reduction was carried out with NRAO ASTRONOMICAL IMAGE PROCESSING SOFTWARE<sup>3</sup> (AIPS; Wells 1985) using standard procedures.

While the nucleus of the host galaxy of SSS17, NGC 4993, was detected and resolved in 1.39 GHz, no significant signal is detected at the position of SSS17a itself. Table 1 summarizes the  $3\sigma$  detection limits, where the r.m.s. level is estimated from source-free regions using the task TVSTAT.

<sup>2</sup> <https://casa.nrao.edu>

<sup>3</sup> <http://www.aips.nrao.edu>

**Table 1.** Log of sub-mm/mm and radio observations of SSS17a.

$T_{\text{start}}$ (UT)	Epoch (day)	Frequency (GHz)	Exposure time (s)	$F_{\nu}$ ( $\mu\text{Jy}$ )
<b>ALMA</b>				
18/08/2017 22:50:40	1.4	338.5	3445	$< 126$
20/08/2017 18:19:35	3.2	338.5	3646	$< 90$
20/08/2017 22:40:16	3.4	338.5	3622	
25/08/2017 22:35:17	8.4	338.5	3445	$< 150$
26/08/2017 22:58:41	9.4	338.5	4480	$< 102$
30/09/2017 15:22:00	44.1	338.5	4237	$< 93$
<b>GMRT</b>				
25/08/2017 09:30:00	7.9	1.39	5400	$< 69$
09/09/2017 11:30:00	23.0	1.39	5400	$< 108$
16/09/2017 07:30:00	29.8	1.39	5400	$< 126$

NOTE—The epoch is with respect to the time of the GW170817.

## 2.3. Other Observations

To augment our data set, we incorporated radio measurements from Corsi et al. (2017a,b,c,d,e), Hallinan et al. (2017), Kaplan et al. (2017), Mooley et al. (2017a,b) (see also Hallinan & others ???), obtained with the Australia Telescope Compact Array (ATCA) and the Very Large Array (VLA). We used the VLA exposure time calculator to convert the relative measurements of Corsi et al. (2017c) and Mooley et al. (2017a) into radio flux densities, adopting r.m.s. values 50% higher than nominal to mitigate possible losses due to antennae problems and adverse observing conditions. We also included the X-ray constraints of Evans et al. (2017) and Haggard et al. (2017a) from the Swift satellite and Chandra X-ray Observatory, as reported in LIGO Scientific Collaboration et al. (2017), as well as optical photometry obtained with the Hubble Space Telescope and ESO’s 8.2-m Very Large Telescope (VLT) by Tanvir et al. (2017a).

## 3. RESULTS AND DISCUSSION

### 3.1. GRB 170817A in the context of other SGRBs

The interaction of the GRB blastwave with the circumburst medium produces an afterglow from X-ray to radio frequencies. The peak of the synchrotron afterglow spectrum is, however, expected to be in the sub-mm/mm band and it rapidly crosses the band towards lower frequencies ( $\nu_{\text{max}} \propto t^{-3/2}$ ; Sari et al. 1998). Our initial ALMA  $3\sigma$  limit of  $F_{338.5\text{ GHz}} < 126 \mu\text{Jy}$  at 1.4 days after GW170817 corresponds to a luminosity of  $3 \times 10^{26} \text{ erg s}^{-1}$  at the redshift of SSS17a. Comparing this estimate for the peak flux of GRB 170817A to estimates of other GRBs from de Ugarte Postigo

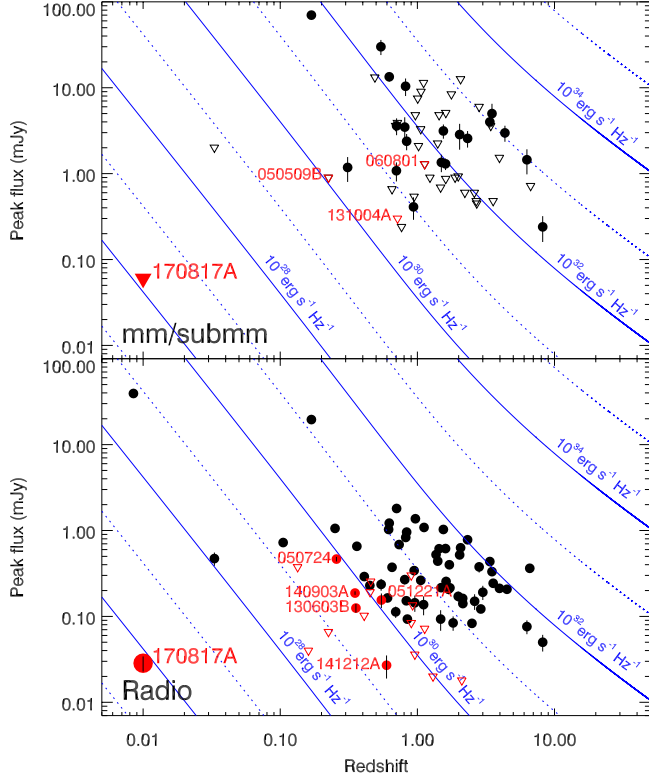


**Figure 1.** Peak flux densities of GRB afterglows derived from mm/sub-mm (top) and radio (bottom) observations. Filled circles and empty triangles denote detections and  $3\sigma$  limits, respectively. SGRBs are shown in red and LGRBs in black. Solid and dotted blue curves indicate equal afterglow luminosities. The non-detection in the sub-mm corresponds to a luminosity limit of  $3 \times 10^{26} \text{ erg s}^{-1} \text{ Hz}^{-1}$ . The faint radio counterpart detected by Corsi et al. (2017c) suggests a peak luminosity of  $\sim 10^{26} \text{ erg s}^{-1} \text{ Hz}^{-1}$ .

et al. (2012) (see Fig. 1, top panel), our sub-mm afterglow limits are  $\sim 3$ – $4$  orders of magnitude fainter than those associated with any long-duration GRBs (LGRBs) or SGRBs.<sup>4</sup>

However, the maximum frequency is also correlated with the energy within the jet and the energy release at  $\gamma$ -rays, e.g.,  $\nu_m \propto E^{1/2}$  for a constant density circumburst medium (Piran 2004). LIGO Scientific Collaboration & Virgo Collaboration (2017a) reported an exceptionally low isotropic-equivalent energy of only  $E_{\gamma, \text{iso}} = (3.08 \pm 0.72) \times 10^{46} \text{ erg}$ . Hence, it is conceivable that the peak of the afterglow spectrum was already in the radio band during our first ALMA observation. To get an additional estimate of the peak luminosity, we use results in Corsi et al. (2017c). Their measurement of  $F_{6\text{GHz}} \sim 28.5 \mu\text{Jy}$  at 28.5 days after GW170817 translates to a luminosity of  $\sim 6.5 \times 10^{25} \text{ erg s}^{-1}$ . Compared to radio mea-

<sup>4</sup> We consider all bursts as SGRBs if the burst duration is  $< 2 \text{ s}$  (observer frame) or if the initial pulse complex lasted less than  $2 \text{ s}$ . In total, 127 *Swift* GRBs, detected until the end of September 2017, fulfill this criterion. Among those 36 have reliable redshifts.

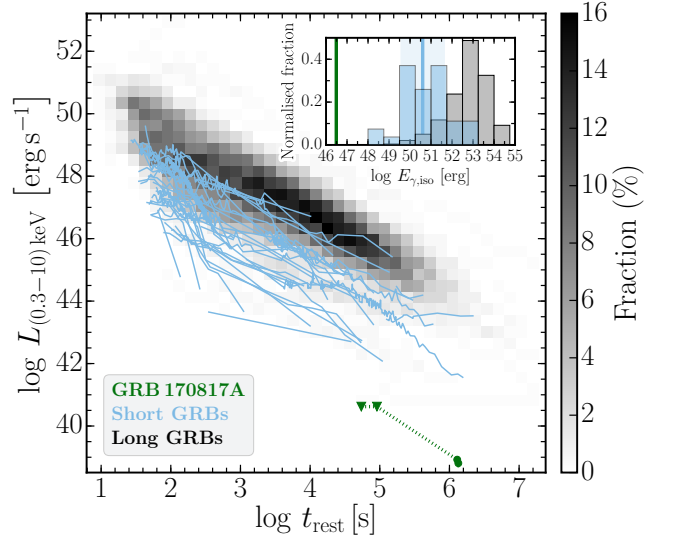


**Figure 2.** X-ray light curves of GRB afterglows. The parameter space occupied by 403 LGRBs, detected between December 2004 and September 2017, is indicated by the density plot. Light curves of 32 SGRBs with detected X-ray afterglows are shown in light blue. GRB170817A lies 2.6 orders of magnitude below the other SGRBs. The inset displays the distribution of energy release at  $\gamma$ -ray energies (SGRBs: blue; LGRBs: grey). The blue vertical line and shaded region indicate the median value and dispersion of the SGRB distribution, respectively.

surements of LGRBs and SGRBs in Fong et al. (2015) and Chandra & Frail (2012), respectively (Fig. 1, bottom panel), the radio afterglow is 2 orders of magnitude fainter than those of LGRBs and SGRBs.

While sub-mm and radio observations are direct tracers of the peak of the afterglow spectrum, only  $\sim 7\%$  of all *Swift* GRBs were bright enough to attempt sub-mm and radio observations. This observational bias is likely to skew the known population towards the bright end of any luminosity function. On the other hand, almost all *Swift* GRBs are detected at X-rays. The mapping between X-ray brightness and the peak of the afterglow spectrum is more complex. It depends on the location of the cooling break, which is usually between the optical and the X-rays, and the density profile of the circumburst medium. Nonetheless, de Ugarte Postigo et al. (2012) showed that X-ray brightness is a useful diagnostic for comparing afterglow luminosities.

Using the measurement reported by Haggard et al. (2017a) in LIGO Scientific Collaboration et al. (2017) we derive a luminosity of  $\sim 8 \times 10^{38} \text{ erg s}^{-1}$  in the rest-frame bandpass from 0.3 to 10 keV at 15.1 days after GW170817. To put this measurement in context of all *Swift* GRBs, we downloaded the X-ray curves of 403 LGRBs and 32 SGRBs with detected X-ray afterglows and known redshift from the *Swift* Burst Analyser (Evans et al. 2010). Identical to Schulze et al. (2014), we computed the rest-frame light curve and resam-



pled the light curves of the LGRB sample on a grid (grey shaded region in Fig. 2). The individual light curves of the SGRB sample are shown in light blue. Similar to the sub-mm and radio, the afterglow is remarkably faint. Already the *Swift* non-detections presented in Evans et al. (2017) reveal that the afterglow is  $> 1.5$  dex fainter than the faintest SGRB with detected afterglow. The deep *Chandra* observation in Haggard et al. (2017a) shows that the GRB was even 2.6 dex fainter than any GRB.

This faintness of the afterglow is also reflected in the very low energy release at  $\gamma$ -rays,  $E_{\gamma, \text{iso}}$ . The observed  $E_{\gamma, \text{iso}}$  distribution of SGRBs and LGRBs is shown in the inset of Fig. 2. The vertical blue line and the shaded region display the median ( $50.88 \pm 0.18$ ) and the sample dispersion ( $0.99^{+0.14}_{-0.12}$ ) of the SGRB sample, computed with the resampling package MULTINEST (Feroz et al. 2013) through its python binding PYMULTINEST (Buchner et al. 2014). With a prompt energy release of  $3.08 \times 10^{46}$  erg (green vertical line the inset of Fig. 2), GRB 170817A was  $\sim 1.5$  dex less energetic than the least energetic SGRB known so far and its deviation from the distribution median has a significance of  $\sim 4.4\sigma$ .

In conclusion, observations of the afterglow revealed an exceptionally underluminous afterglow at all wavelengths at the position of SSS17a. This extremeness is also reflected in the  $\gamma$ -ray properties.

### 3.2. Modeling the broadband afterglow

The previous considerations placed the GRB in the context of long- and short-duration GRBs detected by *Swift*. The discussion neglected the peculiar evolution of the afterglow: non-detection of the afterglow during the first week and its emergence at later epochs. These properties are highly atypical for GRBs, assuming the GRB jet axis is aligned with our line of sight. In the following, we model the observed evolution from X-rays to radio with templates from two-dimensional relativistic hydrodynamical jet simulations using BOXFIT version 2 with the methods described in van Eerten et al. (2012). The templates are generated from a wide range of physical parameters. Here, we use a nine-parameter model:

$$F_{\nu} = L(E_{\text{AG, iso}}, n, \theta_{1/2, \text{jet}}, \theta_{\text{obs}}, p, \epsilon_e, \epsilon_B, \xi_N, z)$$

where  $E_{\text{AG, iso}}$  is the isotropic equivalent energy of the blast-wave (afterglow),  $n$  is the circumburst density at a distance of  $10^{17}$  cm,  $p$  is the power-law index of the electron energy-distribution index,  $\theta_{1/2, \text{jet}}$  is the jet half-opening angle,  $\theta_{\text{obs}}$  is the observer/viewing angle,  $\epsilon_e$  and  $\epsilon_B$  are the fractions of the internal energy in the shock-generated magnetic field and electrons, respectively, and  $\xi_N$  is the fraction of electrons that are accelerated and  $z$  is the redshift.

We fix the fractions of  $\epsilon_e$  and  $\xi_N$  at 0.1 and 1, respectively, and  $p$  to 2.43 and the redshift to 0.009854. The other parameters are varied within the following ranges:  $\theta_{1/2, \text{jet}} = 5^{\circ} - 45^{\circ}$ ,

$E_{\text{AG, iso}} = 10^{47} - 10^{53}$  erg,  $\epsilon_B = 10^{-5} - 10^{-2}$ ,  $n = 10^{-4} - 10^{-1} \text{ cm}^{-3}$  and  $\theta_{\text{obs}} = 0^{\circ} - 45^{\circ}$ . The afterglow was modeled in a homogeneous ISM environment and we apply this model to eight representative frequencies: 1.4, 3, 6, 21, 338.5 GHz as well as the optical filters *F606W* and *F475W* and X-rays at 3 keV.

A critical aspect of the off-axis afterglow modeling is the resolution in azimuthal direction, in particular for models with large  $\theta_{\text{obs}}$  to  $\theta_{1/2, \text{jet}}$  ratios. We chose a numerical resolution of 20 and 30, for  $\theta_{1/2, \text{jet}} > 9^{\circ}$  and  $\theta_{1/2, \text{jet}} < 9^{\circ}$ , respectively. Comparisons to simulations with a numerical resolution in azimuthal direction of 70 show that the lower resolution templates accurately capture the temporal evolution of the afterglow and they are also able to recover the absolute flux scale at maximum to within 20%. The maximum flux of models with very narrow jet are recovered less accurately in off-axis afterglow models. As we show below, these models are not adequate to describe the observed afterglow evolution independent of the issue on the absolute flux scale. The numerical resolution in azimuthal direction was set to unity if the viewing angle is negligible, as suggested by the BOXFIT manual.

The gray curves in Fig. 3 display a set of strict on-axis afterglow models (i.e.,  $\theta_{\text{obs}} = 0$ ) with a half-opening angle of  $5^{\circ}$ ,  $\epsilon_B = 0.01$ ,  $n = 10^{-2} \text{ cm}^{-2}$ , and for  $E_{\text{AG, iso}}$  between  $10^{48}$  and  $10^{53}$  erg. Common to on-axis afterglow models ( $\theta_{\text{obs}} < \theta_{1/2, \text{jet}}$ ) is the strict monotonic decline in X-rays and the optical, whereas the radio can exhibit a plateau or an initial rise. This evolution is in stark contrast to observations of SSS17a. The best-matching templates (colored curves in Fig. 3) strongly argues for a GRB seen off-axis (i.e.,  $\theta_{\text{obs}} > \theta_{1/2, \text{jet}}$ ; possible off-axis LGRB candidates were discussed in Fynbo et al. 2004; Guidorzi et al. 2009; Krühler et al. 2009).

*Model 1* (thin curves in Fig. 3) favors an afterglow with an energy reservoir of  $\sim 10^{50}$  erg and a magnetic equipartition fraction of  $\epsilon_B \sim 10^{-2}$ , and a moderately collimated outflow with a half-opening angle of  $\theta_{1/2, \text{jet}} \sim 20^{\circ}$ , traversing a circumburst medium with a density of  $10^{-2} \text{ cm}^{-2}$ . The jet axis and the line of sight are misaligned by  $41^{\circ}$ . *Model 2* (thick curves in Fig. 3) suggests a more collimated, more powerful jet with  $\theta_{1/2, \text{jet}} \sim 5^{\circ}$ ,  $E_{\text{AG, iso}} \sim 10^{51}$  erg and  $\epsilon_B \sim 2 \times 10^{-3}$ , traversing a more tenuous circumburst medium ( $n \sim 5 \times 10^{-4} \text{ cm}^{-3}$ ). In this scenario, the line of sight and the GRB jet axis are misaligned by  $17^{\circ}$ .

The inferred afterglow properties are in both cases very close to the average values of SGRBs in Fong et al. (2015), corroborating that this GRB is *not* different from the population of known SGRBs. To break degeneracies, more detections are required. Reassuringly, the derived viewing angles are consistent with the conservative limit of  $< 56^{\circ}$  from the GW signal. Moreover the narrow jet template (*Model 2*) is consistent with the even stricter LIGO limit of  $< 31^{\circ}$  (LIGO Scientific Collaboration & Virgo Collaboration 2017b).

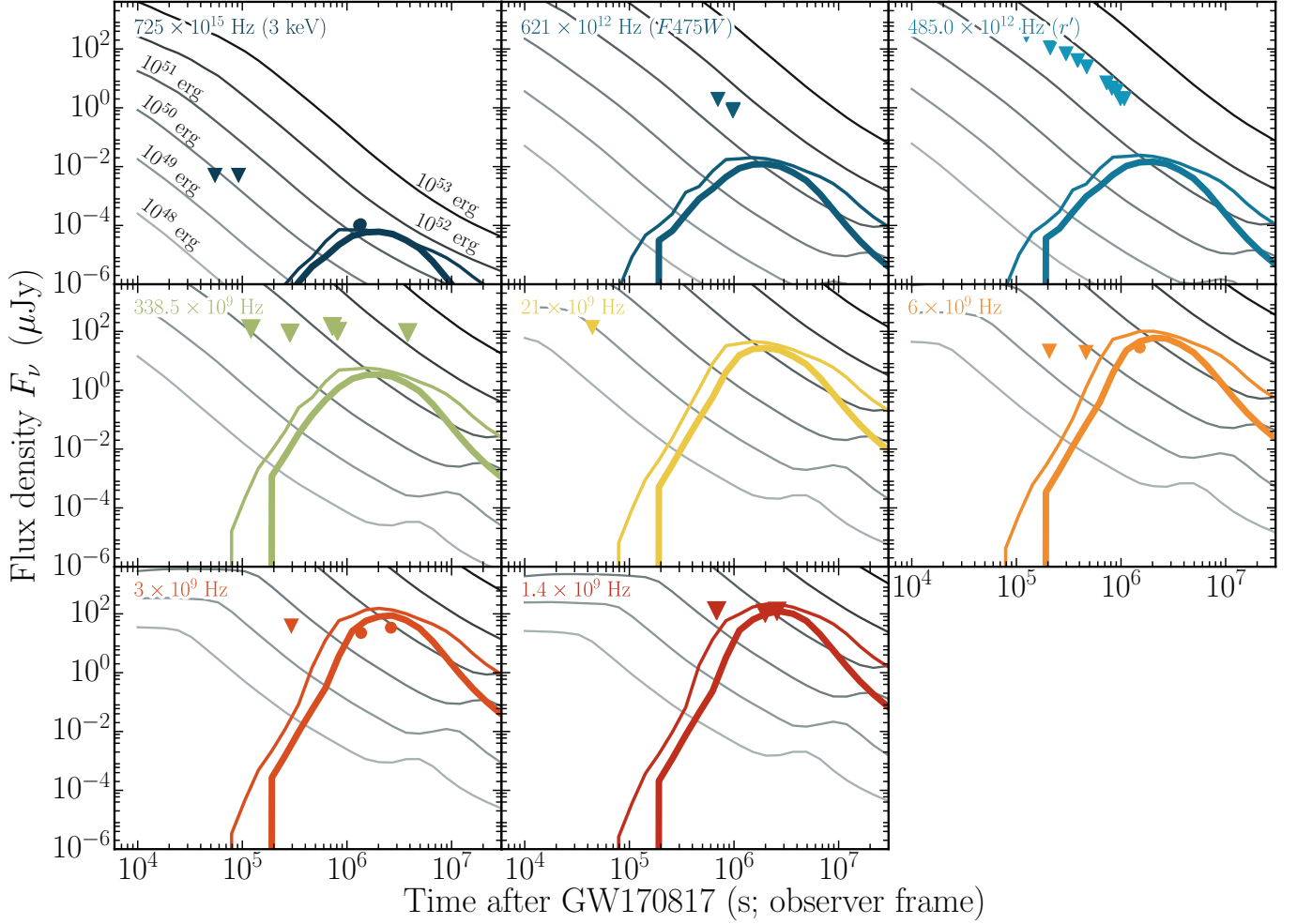


**Figure 3.** The afterglow from radio to X-ray frequencies (detections:  $\bullet$ ; non-detections:  $\blacktriangledown$ ; our ALMA and GMRT measurements are displayed slightly larger.). The light curves are adequately modeled with two distinct templates: *model 1* –  $E_{\text{AG, iso}} \sim 10^{50}$  erg,  $\theta_{1/2, \text{jet}} \sim 20^\circ$ ,  $\theta_{\text{obs}} \sim 41^\circ$ ,  $n \sim 10^{-2} \text{ cm}^{-3}$ , and  $\epsilon_B \sim 10^{-2}$  (thin curves); *model 2* –  $E_{\text{AG, iso}} \sim 10^{51}$  erg,  $\theta_{1/2, \text{jet}} \sim 5^\circ$ ,  $\theta_{\text{obs}} \sim 17^\circ$ ,  $n \sim 5 \times 10^{-4} \text{ cm}^{-3}$ , and  $\epsilon_B \sim 2 \times 10^{-3}$  (thick curves). The grey curves show the evolution of an on-axis afterglow with  $\theta_{1/2, \text{jet}} = 5^\circ$ ,  $\theta_{\text{obs}} = 0^\circ$ ,  $n = 10^{-2} \text{ cm}^{-3}$ , and  $\epsilon_B = 10^{-2}$ . The energy of the afterglow was varied between  $10^{48}$  and  $10^{53}$  erg, indicated by the grey-scale color pattern. Combining the non-detections at early times and the detections at late-times rules out the entire parameter space of on-axis afterglow models. The rebrightening seen in some on-axis models at  $> 10^6$  s is due to the contribution of the GRB counter-jet. For a detailed discussion see §3.2.

With the best-match templates in hand, we quantify the contamination of the kilonova by the afterglow. The upper panels in Fig. 3 display the light curve in *F475W* ( $6.2 \times 10^{12}$  Hz) and *r'/F606W* ( $4.9 \times 10^{12}$  Hz) by Tanvir et al. (2017a). The contamination by the afterglow in the optical is negligible ( $< 1\%$ ) during the week after GW170817 for both afterglows. Hence the inferred KN properties in Tanvir et al. (2017a) and all other papers on SSS17a do not require any afterglow correction.

### 3.3. Inferring jet parameters from $\gamma$ -ray and afterglow emission

For an off-axis observer, the observed isotropic  $\gamma$ -ray energy  $E_{\gamma, \text{iso}}$  depends on  $\theta_{1/2, \text{jet}}$ ,  $\theta_{\text{obs}}$ , the initial bulk Lorentz factor of the jet  $\Gamma_0$ , and the beaming-corrected energy release

in  $\gamma$ -rays ( $E_\gamma$ ). Similarly, the true and observed  $E_{\text{peak}}$  values are also related through  $\theta_{1/2, \text{jet}}$ ,  $\theta_{\text{obs}}$  and  $\Gamma_0$ . In the following, we use analytical expressions relating these parameters under the ambit of the uniform top-hat jet model (Donaghy 2006) that agree very well with the numerical calculations for off-axis jets in Yamazaki et al. (2003a,b). In this prescription, for a given  $\theta_{1/2, \text{jet}}$  and  $E_\gamma$ , the  $E_{\gamma, \text{iso}}$  measured by the off-axis observer at  $\theta_{\text{obs}}$  can be expressed as a function of  $\Gamma_0$ . The observed  $E_{\text{peak}}$  can also be expressed in a similar way as function of the on-axis  $E_{\text{peak}}$  and  $\Gamma_0$  for a fixed  $\theta_{1/2, \text{jet}}$  and  $\theta_{\text{obs}}$ .

We use the best-fit  $\theta_{1/2, \text{jet}}$  and  $\theta_{\text{obs}}$  from two models that agree well with the afterglow data (*model 1*: wide jet; *model 2*: narrow jet) along with the prompt emission energetics from *Fermi* to infer the bulk Lorentz factor  $\Gamma_0$  of the jet. We

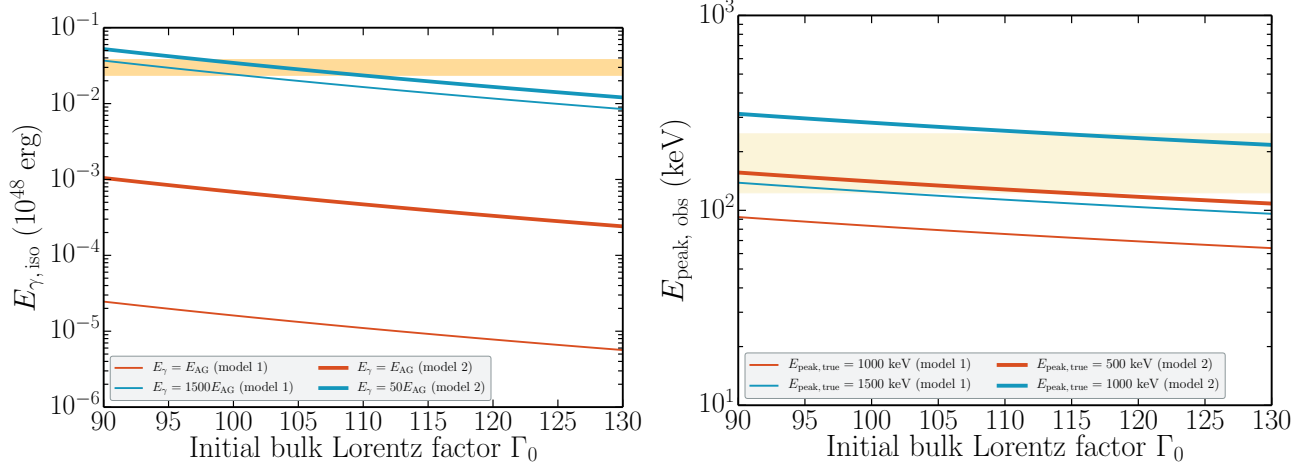


**Figure 4.** The observed isotropic  $\gamma$ -ray energy release and the observed  $E_{\text{peak}}$  of the prompt emission as a function of  $\Gamma_0$ . The Fermi observations are indicated as the yellow band. We have used our best fit  $\theta_{1/2,\text{jet}}$  and  $\theta_{\text{obs}}$  from both the models in the calculation.

consider the  $E_{\text{AG},\text{iso}}$  of the blast wave from afterglow modeling as a proxy for  $E_{\gamma,\text{iso}}$ .

In the wide-jet scenario from §3.2 (*model 1*),  $E_{\gamma,\text{iso}}$  is required to be a factor of 1500 larger than the energy deposited in the afterglow to be consistent with observations (Fig. 4, left panel, thin blue line). However, such an excessively high value is unheard of in the sample in Cenko et al. (2011). Moreover, such a scenario would also require a peak energy of 1.5 MeV during the  $\gamma$ -ray burst (Fig. 4, right panel), which would be at the upper end of the peak-energy distribution of GRBs detected by *Fermi*/GBM and CGRO/BATSE (e.g., Nava et al. 2011). A more common  $E_{\gamma,\text{iso}}/E_{\text{AG},\text{iso}}$  ratio between 1 and 10 (thin blue line in (Fig. 4) would be inconsistent with observations of GRB 170817A (shaded regions in Fig. 4). In the narrow-jet scenario from §3.2 (*model 2*), we find that an  $E_{\gamma,\text{iso}} \sim 50 \times E_{\text{AG},\text{iso}}$  is required to reproduce the observed (off-axis) *Fermi*  $E_{\gamma,\text{iso}}$  (Fig. 4, thick red curve) with  $\Gamma_0 \sim 100$ . For lower values of  $E_{\gamma,\text{iso}}$ , the required bulk Lorentz factor is reduced. A ratio of  $\sim 50$  between the prompt to afterglow energy release is not unheard of (Cenko et al. 2011). For similar  $\Gamma_0$  values, we find that an on-axis observer would have seen GRB 170817A with a  $E_{\text{peak}}$  of 500 keV (Fig. 4).

### 3.4. Low frequency radio emission from merger ejecta

Non-relativistic shocks from the merger ejecta are thought to emit at radio frequencies (Nakar & Piran 2011). This model predicts that the emission peaks in the MHz regime and at the epoch of deceleration of the non-relativistic shock, which is expected to be of the orders of months to years after the merger.

To examine whether this mechanism could produce a bright transient months after GW170817, we use the observed properties of the kilonova and the afterglow. The

expected brightness in optically thin GHz frequencies would be,

$$f_\nu(t) = 655 \text{ mJy } n_0^{1.8} \frac{R(t)^3}{10^{17}} \beta(t)^{3.75} \epsilon_B^{0.78} \epsilon_e \left( \frac{\nu}{\text{GHz}} \right)^{-0.55},$$

for a  $p = 2.1$ ; where  $R(t)$  is the radius of the shock front (normalized to  $10^{17}$  cm) and  $\beta(t)$  is the normalized velocity. Radius and the observed time  $t$  are related through  $R = \beta ct$ . The epoch of deceleration, where the swept-up mass equals the ejected mass, is given by  $t_{\text{dec}} = 7 \text{ yr} \left( \frac{M_{\text{ej},\odot}}{n_0} \right)^{1/3} \beta_0^{-1}$ , where  $\beta_0$  is the normalized initial velocity.

Tanvir et al. (2017b) concluded that the merger ejected  $\sim 5 \times 10^{-4} M_\odot$  with velocity of  $0.1 c$ . Along with a circumburst medium density,  $n = 0.01 \text{ cm}^{-3}$ , we estimate the brightness in L band to be  $\sim 60 \mu\text{Jy}$  for a deceleration time scale of 55 years. A smaller ambient density will further reduce the flux and increase the  $t_{\text{dec}}$ . Therefore, the outlook assuming this model is valid is bleak.

The merger remnant, if a magnetar, can inject additional energy into the shock (Metzger & Bower 2014). This excess energy will also delay  $t_{\text{dec}}$ . In this model, from the observed  $\beta$  and best-fit ambient density,  $t_{\text{dec}} = 260 E_{\text{mag},52} \text{ yr}$ , where  $E_{\text{mag},52}$  is the energy input from the magnetar. The peak flux in L band at  $t_{\text{dec}} \sim 3 \text{ mJy}$  for our parameters, which like in the previous case scales down as a  $t^3$  power-law to the current epoch. Therefore we do not expect any detectable emission at GMRT frequencies at present from the merger ejecta, consistent with our observations.

## 4. SUMMARY

LIGO/Virgo detected a BNSM at a distance of  $\sim 40 \text{ Mpc}$  on 17 August 2017. Rapid optical and near-IR follow-up observations detected a new transient, SSS17a, in the credible region of GW170817 with properties consistent with



KN models. Gamma-ray satellites detected the short GRB 170817A quasi-contemporaneously with GW170817, but owing to the poor localization at  $\gamma$ -rays this did not exclude a chance alignment.

We observed the position of SSS17a with ALMA and GMRT at 338.5 and 1.4 GHz, respectively, from 1.4 days to 44 days after the merger, our objective being to constrain the GRB afterglow component. The afterglow evaded detection at all epochs. Our radio and sub-mm observations allow us to place a firm upper limit of a few  $10^{26}$  erg s $^{-1}$  in the sub-mm and radio, probing a regime  $> 2$ –4 orders of magnitudes fainter than previous limits on SGRBs.

The emergence of an X-ray and radio transient at the position of SSS17a at 9 and 17 days after GW170817, respectively, is highly atypical for GRBs. Modeling the evolution from radio to X-ray frequencies with templates generated from 2D relativistic hydrodynamical jet simulations exclude all on-axis afterglow models ( $\theta_{1/2, \text{jet}} > \theta_{\text{obs}}$ ) with sensible physical parameters. Adequate models, describing the evolution from X-ray to radio frequencies, require strict off-axis afterglow templates where  $\theta_{1/2, \text{jet}} < \theta_{\text{obs}}$ . *Model 1* favors a jet, powered by  $E_{\text{AG, iso}} \sim 10^{50}$  erg, with magnetic equipartition of  $\epsilon_B \sim 10^{-2}$  and an initial half-opening angle of  $\sim 20^\circ$ , traversing a circumburst medium with  $n = 10^{-2}$  cm $^{-3}$ . The second model suggests a more collimated and more powerful jet:  $E_{\text{AG, iso}} \sim 10^{51}$  erg,  $\theta_{1/2, \text{jet}} \sim 5^\circ$ ,  $\epsilon_B = 2 \times 10^{-3}$ ,  $n = 5 \times 10^{-4}$  cm $^{-3}$ . More detections of the afterglow are needed to reduce the degeneracy in the model parameters. In both cases our line of sight and the GRB jet axis were misaligned by  $\sim 41^\circ$  (wide-jet model) and  $\sim 20^\circ$  (narrow jet model), explaining the emergence of the afterglow only a week after the GRB. The viewing angle measurements are consistent with upper limits by [LIGO Scientific Collaboration & Virgo Collaboration \(2017b\)](#).

The jet parameters are, in both cases, consistent with mean values of the *Swift* SGRB population. Using  $\theta_{1/2, \text{jet}}$ ,  $\theta_{\text{obs}}$ , and  $E_{\text{iso}}$  of the blast wave, we inferred the true  $\gamma$ -ray energy release and initial bulk Lorentz factor ( $\Gamma_0$ ) of the flow. The two parameters are correlated. We find that for  $\Gamma_0 \sim 100$ , the prompt energy release has to be at least an order of magnitude higher than the kinetic energy in the afterglow. For similar  $\Gamma_0$ , an on-axis observer would have seen this burst

with  $E_{\text{peak}} \sim 500$ –1000 keV consistent with the *Fermi* on-axis SGRB sample.

Using the best-match template we assessed if the afterglow contaminated significantly the KN optical emission. The contamination is  $< 1\%$  during the first week after GW170817. We also calculated the expected radio emission from the merger ejecta and found it to be negligible presently.

The afterglow modeling allows us to draw the following conclusions: *i*) this is the first robust detection of an off-axis GRB with  $\theta_{\text{obs}} > \theta_{1/2, \text{jet}}$  and *ii*) SSS17a and GRB 170817A have the same progenitor. These findings in conjunction with the spectroscopic evidence for lanthanide elements in spectra of SSS17a (e.g., [Pian et al. 2017](#); [Smartt et al. 2017](#)), demonstrate that some SGRBs are connected with BNSMs and firmly establishes that SSS17a and GRB 170817A are the electromagnetic counterpart to GW170817.

ALMA is a partnership of ESO (representing its member states), NSF (USA) and NINS (Japan), together with NRC (Canada), MOST and ASIAA (Taiwan), and KASI (Republic of Korea), in cooperation with the Republic of Chile. The Joint ALMA Observatory is operated by ESO, AUI/NRAO and NAOJ. The GMRT is run by the National Center for Radio Astrophysics of the Tata Institute of Fundamental Research. L. Resmi thanks Suma Murthy, Anandmayee Tej, Swagat R. Das, and Jagadheep D. Pandian for discussions on radio interferometric analysis. This work made use of data supplied by the UK *Swift* Science Data Centre at the University of Leicester.

Development of the Boxfit code was supported in part by NASA through grant NNX10AF62G issued through the Astrophysics Theory Program and by the NSF through grant AST-1009863. Simulations for BOXFIT version 2 have been carried out in part on the computing facilities of the Computational Center for Particle and Astrophysics (C2PAP) of the research cooperation "Excellence Cluster Universe" in Garching, Germany.

*Facilities:* ALMA, GMRT

*Software:* AIPS, Boxfit, CASA, MultiNest, PyMultiNest

## REFERENCES

- Abadie, J., Abbott, B. P., Abbott, R., et al. 2010, [Classical and Quantum Gravity](#), **27**, 173001
- Abbott, B. P., Abbott, R., Abbott, T. D., et al. 2016, [Physical Review Letters](#), **116**, 241102
- Alexander, K., et al. 2017, GCN Circular, 21589
- Allam, S., et al. 2017, GCN Circular, 21530
- Bannister, K., Lynch, C., Kaplan, D., & Murphy, T. 2017, GCN Circular, 21537
- Berger, E. 2014, [ARA&A](#), **52**, 43
- Blackburn, L., Briggs, N. S., Broida, J., et al. 2017, GCN Circular, 21506
- Buchner, J., Georgakakis, A., Nandra, K., et al. 2014, [A&A](#), **564**, A125

- Cenko, S. B., Frail, D. A., Harrison, F. A., et al. 2011, *ApJ*, **732**, 29
- Cenko, S. B., et al. 2017, GCN Circular, 21572
- Chandra, P., & Frail, D. A. 2012, *ApJ*, **746**, 156
- Corsi, A., et al. 2017a, GCN Circular, 21664
- . 2017b, GCN Circular, 21613
- . 2017c, GCN Circular, 21815
- . 2017d, GCN Circular, 21636
- . 2017e, GCN Circular, 21614
- Coulter, D. A., et al. 2017, GCN Circular, 21529
- De, K., et al. 2017, GCN Circular, 21708
- de Ugarte Postigo, A., Lundgren, A., Martín, S., et al. 2012, *A&A*, **538**, A44
- Deller, A., et al. 2017, GCN Circular, 21588
- Donaghy, T. Q. 2006, *ApJ*, **645**, 436
- Eichler, D., Livio, M., Piran, T., & Schramm, D. N. 1989, *Nature*, **340**, 126
- Einstein, A. 1916, Sitzungsberichte der Königlich Preußischen Akademie der Wissenschaften (Berlin), 688
- . 1918, Sitzungsberichte der Königlich Preußischen Akademie der Wissenschaften (Berlin), 154
- Evans, P., et al. 2017, GCN Circular, 21550
- Evans, P. A., Cenko, S. B., Kennea, J. A., & et al. 2017, *Science*, in press, doi:10.1126/science.aap9580
- Evans, P. A., Willingale, R., Osborne, J. P., et al. 2010, *A&A*, **519**, A102
- Feroz, F., Hobson, M. P., Cameron, E., & Pettitt, A. N. 2013, ArXiv e-prints, [arXiv:1306.2144 \[astro-ph.IM\]](https://arxiv.org/abs/1306.2144)
- Fong, W., Berger, E., Margutti, R., & Zauderer, B. A. 2015, *ApJ*, **815**, 102
- Fong, W., Margutti, R., & Haggard, D. 2017, GCN Circular, 21786
- Fynbo, J. P. U., Sollerman, J., Hjorth, J., et al. 2004, *ApJ*, **609**, 962
- Goldstein, A., et al. 2017a, *ApJ*, in press, doi:10.3847/2041-8213/aa8f41
- . 2017b, GCN Circular, 21528
- Guidorzi, C., Clemens, C., Kobayashi, S., et al. 2009, *A&A*, **499**, 439
- Haggard, D., et al. 2017a, *ApJ*, in press, doi:10.3847/2041-8213/aa8ede
- . 2017b, GCN Circular, 21798
- Hallinan, G., Corsi, C., Mooley, K., Frail, D. A., & Kasliwal, M. 2017, GCN Circular, 21929
- Hallinan, G., et al. ????
- Hjorth, J., et al. 2017, *ApJL*, **848**, L31
- Jin, Z.-P., Li, X., Cano, Z., et al. 2015, *ApJL*, **811**, L22
- Jin, Z.-P., Hotokezaka, K., Li, X., et al. 2016, *Nature Communications*, **7**, 12898
- Kaplan, D., et al. 2017, GCN Circular, 21574
- Kasen, D., Badnell, N. R., & Barnes, J. 2013, *ApJ*, **774**, 25
- Krühler, T., Greiner, J., Afonso, P., et al. 2009, *A&A*, **508**, 593
- Levan, A. J., Lyman, J. D., Tanvir, N. R., et al. 2017, *ApJL*, in press, doi: 10.3847/2041-8213/aa905f
- Li, L.-X., & Paczyński, B. 1998, *ApJ*, **507**, L59
- LIGO Scientific Collaboration, & Virgo Collaboration. 2017a, Discovery of a Short Gamma-Ray Burst Associated with a Binary Neutron Star Merger, Tech. rep.
- . 2017b, *PhRvL*, accepted, 10.1103/PhysRevLett.119.161101
- LIGO Scientific Collaboration, Virgo Collaboration, & Partner Astronomy Groups. 2017, *ApJL*, in press, doi:10.3847/2041-8213/aa91c9
- Margutti, R., Fong, W., Berger, E., et al. 2017, GCN Circular, 21648
- McMullin, J. P., Waters, B., Schiebel, D., Young, W., & Golap, K. 2007, in *Astronomical Society of the Pacific Conference Series*, Vol. 376, *Astronomical Data Analysis Software and Systems XVI*, ed. R. A. Shaw, F. Hill, & D. J. Bell, 127
- Melandri, A., et al. 2017, GCN Circular, 21532
- Metzger, B. D. 2017, *Living Reviews in Relativity*, **20**, 3
- Metzger, B. D., & Bower, G. C. 2014, *Mon. Not. Roy. Astron. Soc.*, **437**, 1821
- Mooley, K. P., et al. 2017a, GCN Circular, 21814
- . 2017b, GCN Circular, 21650
- Nakar, E. 2007, *PhR*, **442**, 166
- Nakar, E., & Piran, T. 2011, *Nature*, **478**, 82
- Nava, L., Ghirlanda, G., Ghisellini, G., & Celotti, A. 2011, *MNRAS*, **415**, 3153
- Pian, E., et al. 2017, *Nature*, in press, doi:10.1038/nature24298
- Piran, T. 2004, *Reviews of Modern Physics*, **76**, 1143
- Planck Collaboration. XVI. 2014, *A&A*, **571**, A16
- Resmi, L., Misra, M., Tanvir, N. R., O'Brian, P., & Schulze, S. 2017, GCN Circular, 21768
- Rosswog, S. 2005, *ApJ*, **634**, 1202
- Sari, R., Piran, T., & Narayan, R. 1998, *ApJL*, **497**, L17
- Savchenko, V., et al. 2017a, *ApJ*, in press, doi:10.3847/2041-8213/aa8f94
- . 2017b, GCN Circular, 21507
- Schulze, S., Malesani, D., Cucchiara, A., et al. 2014, *A&A*, **566**, A102
- Schulze, S., et al. 2017, GCN Circular, 21747
- Smartt, S. J., et al. 2017, *Nature*, 10.1038/nature24303
- Sugita, S., Kawai, N., Serino, M., et al. 2017, GCN Circular, 21555
- Swarup, G., Ananthakrishnan, S., Kapahi, V. K., et al. 1991, *Current Science*, **60**, 95
- Tanaka, M., Hotokezaka, K., Kyutoku, K., et al. 2014, *ApJ*, **780**, 31
- Tanvir, N. R., & Levan, A. J. 2017, GCN Circular, 21544
- Tanvir, N. R., Levan, A. J., Fruchter, A. S., et al. 2013, *Nature*, **500**, 547
- Tanvir, N. R., Levan, A. J., Gonzales-Fernandez, C., et al. 2017a, *ApJ*, in press, doi:10.3847/2041-8213/aa90b6
- Tanvir, N. R., et al. 2017b, *ApJL*, submitted

- Troja, E., et al. 2017, GCN Circular, 21765
- van Eerten, H., van der Horst, A., & MacFadyen, A. 2012, [ApJ](#), 749, 44
- von Kienlin, A., Meegan, C., & Goldstein, A. 2017, GCN Circular, 21520
- Wells, D. C. 1985, in *Data Analysis in Astronomy*, ed. V. di Gesu, L. Scarsi, P. Crane, J. H. Friedman, & S. Levialdi, 195
- Wooten, A., & Thompson, A. R. 2009, [IEEE Proceedings](#), 97, 1463
- Yamazaki, R., Ioka, K., & Nakamura, T. 2003a, [ApJ](#), 593, 941
- Yamazaki, R., Yonetoku, D., & Nakamura, T. 2003b, [ApJ](#), 594, L79
- Yang, S., Valenti, S., Sand, D., et al. 2017, GCN Circular, 21531